


Shear viscosity of bimodal capsule suspensions in simple shear flow

Hiroki Ito

Graduate School of Biomedical Engineering, Tohoku University, Japan

Daiki Matsunaga

Graduate School of Engineering Science, Osaka University, Japan

Yohsuke Imai *

Graduate School of Engineering, Kobe University, Japan



(Received 9 August 2018; published 7 November 2019)

We present a numerical analysis of the shear viscosity of bimodal suspensions in Stokes flow. The dynamics of capsules whose membrane follows Skalak law is simulated for the total volume fraction $\phi = 0.4$. A suspension of two types of capsules with different sizes and the same deformability (capillary number) has a decreased shear viscosity compared to monomodal suspensions. Increasing the deformability of the capsules amplifies the extent of the viscosity reduction. The viscosity reduction is mainly caused by a decrease in the shear component of the stresslet of the large capsules, due to a decrease in their deformation and orientation angle with respect to the flow direction. In the case of a suspension of two types of capsules with the same size and different deformabilities, the shear viscosity is nearly the same as the weighted average of monomodal suspensions. An increase in the stresslet of the floppy capsules is counterbalanced by a decrease in the stresslet of the stiff capsules. For a suspension of two types of capsules with different sizes and the same membrane stiffness, the effects of the size difference and deformability difference coexist. The interplay of these effects decreases the stresslet for both the large and small capsules, resulting in a further viscosity reduction.

DOI: [10.1103/PhysRevFluids.4.113601](https://doi.org/10.1103/PhysRevFluids.4.113601)

I. INTRODUCTION

A particle consisting of an inner fluid surrounded by a thin elastic membrane is called a capsule. Capsules are found in diverse applications, such as bioengineering, chemical engineering, pharmaceutical science, and food science. Various studies have been conducted to understand the motion and deformation of capsules and the suspension rheology [1]. A spherical capsule in shear flow deforms into an ellipsoidal shape in response to hydrodynamic forces, and particle stress is generated by the deformation [2]. Due to the deformability of capsules, capsule suspensions exhibit rheological behaviors different from those of rigid-particle suspensions. Typical examples include shear thinning behavior and a positive first normal stress difference [3–7]. When the volume fraction of the capsules increases, hydrodynamic interactions between the capsules increase the shear viscosity nonlinearly [8,9], similar to rigid-particle suspensions. However, the effect of high-order terms is suppressed by the interplay between the deformation and orientation of the capsules [10].

In past rheological analyses of capsule suspensions, most studies assumed that all capsules have the same physical properties, but in reality, each capsule may have unique physical properties. For example, a size distribution may be present in the production process of artificial capsules [11]. However, the rheology of such suspensions of multimodal capsules is not yet understood. For

*yimai@mech.kobe-u.ac.jp

rigid-particle suspensions, various studies have been conducted to examine the effect of the particle size distribution on the suspension rheology. The characteristic rheological behavior of bimodal suspensions of rigid spheres is a reduction in shear viscosity. At a fixed total volume fraction, the shear viscosity is lower for a bimodal suspension than a monomodal suspension; hence, the shear viscosity is minimized at some non-zero value of the relative volume fraction of small particles [12,13]. The extent of the viscosity reduction is amplified when the total volume fraction increases or the size difference between two sizes of particles increases. The normal stress difference also decreases in bimodal suspensions [14]. The viscosity reduction is often linked to the maximum packing fraction of particles [14–16], and empirical models have been proposed to predict the viscosity of bimodal suspensions [17].

If particles are given the ability to deform, is the extent of the viscosity reduction suppressed or amplified? Here we show that increasing the deformability of capsules amplifies the extent of the viscosity reduction. A shear viscosity reduction has also been observed in bimodal emulsions [18–20]. In the case of emulsions, the deformability of drops is given by the capillary number, $Ca = \mu\dot{\gamma}a/\sigma$, where μ is the viscosity of the outer fluid, $\dot{\gamma}$ is the shear rate, a is the radius of drops, and σ is the surface tension. Because of the constant surface tension of drops, two types of drops with different sizes must also have different deformabilities, as expressed by the difference in their capillary numbers. In this study, we investigate the shear viscosity of bimodal suspensions of capsules. The deformability of capsules is determined by $Ca = \mu\dot{\gamma}a/G$, where G represents the membrane stiffness, called the surface shear elastic modulus. When two types of capsules have the same surface shear elastic modulus, bimodal capsule suspensions resemble bimodal emulsions: small and large capsules have different deformabilities. For a better understanding of bimodal capsule suspensions, the separate effects of the size and deformability differences on the shear viscosity should be clarified. For this purpose, we first analyze the shear viscosity of a suspension of two types of capsules with different sizes and the same deformability. The analysis is then extended to a suspension of capsules with the same size and different deformabilities, and finally, a suspension of capsules with different sizes and the same membrane stiffness is discussed. The viscosity ratio between the inner and outer fluids also affects the capsule deformability. However in this study, we concentrate on the size ratio and the capillary number ratio and fix the viscosity ratio to be 1. Simple cases under this assumption could be the limitation of this study but could give a fundamental understanding of bimodal capsule suspensions.

II. PROBLEM STATEMENT AND NUMERICAL METHOD

A. Problem statement

Consider two types of capsules, type A and type B, suspended in a Newtonian fluid of viscosity μ . The particle Reynolds number is assumed to be much less than unity. Both types of capsules are neutrally buoyant, and their inner fluids have the same viscosity as the outer fluid. We apply a simple shear flow of shear rate $\dot{\gamma}$ for an infinite periodic domain.

We fix the total volume fraction of the capsules to be $\phi = \phi^A + \phi^B = 0.4$. The relative volume fraction of type B capsules to the total volume fraction is denoted by $R_\phi = \phi^B/\phi$. The capsules of type A have a radius a^A and a surface shear elastic modulus G^A for the membrane, and capsules of type B have respective values a^B and G^B . The capsules are characterized by their size and membrane stiffness, with the ratio of their radii and surface shear elastic moduli defined as $R_a = a^B/a^A$ and $R_G = G^B/G^A$, respectively. However, the deformability of a capsule depends not only on the membrane stiffness but also on the size of the capsule. The capsule deformability is therefore characterized by the capillary number, $Ca = \mu\dot{\gamma}a/G$, and the capillary number ratio is defined by $R_{Ca} = Ca^B/Ca^A$. Note that the capillary number ratio can also be written as $R_{Ca} = R_a/R_G$.

We investigate three categories of bimodal suspensions (Fig. 1): two types of capsules with different sizes and the same deformability, $R_a \neq 1$ and $R_{Ca} = 1$; two types of capsules with the same size and different deformabilities, $R_a = 1$ and $R_{Ca} \neq 1$; and two types of capsules with different sizes and the same membrane stiffness, $R_a \neq 1$ and $R_G = 1$, or $R_{Ca} = R_a$.

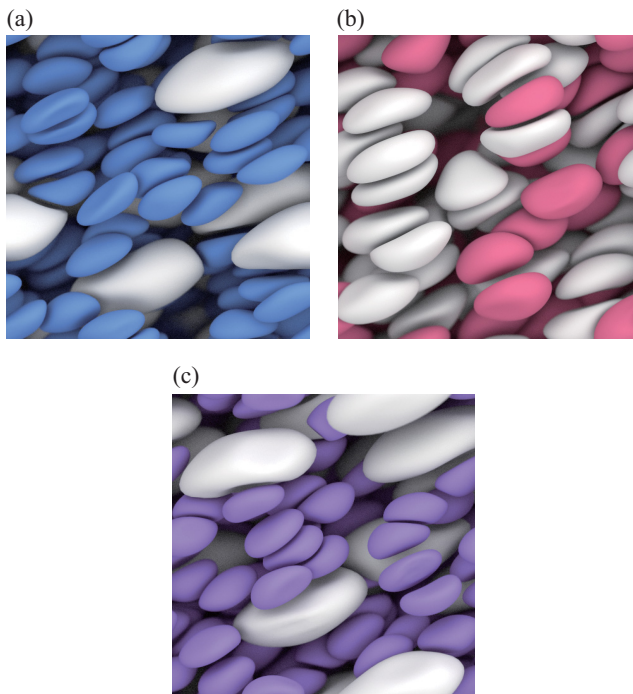


FIG. 1. Three categories of bimodal capsule suspensions. (a) $R_a \neq 1$ and $R_{Ca} = 1$, (b) $R_a = 1$ and $R_{Ca} \neq 1$, (c) $R_a \neq 1$ and $R_{Ca} = R_a$.

The capillary number may range from $O(10^{-2})$ to $O(10^1)$ in experiments (for example, see Gubspun *et al.* [21] and de Loubens *et al.* [22]). Here we examine three values of the capillary number: $Ca^A = 0.4, 1.0$, and 2.4 with an area dilation coefficient $C = 1$ [see also Eq. (5)]. Note that we do not intend to directly model a specific case of real suspensions and systematically vary the parameter range to gain a fundamental understanding of bimodal capsule suspensions.

B. Governing equations

The velocity \mathbf{v} at the position \mathbf{x} is described by the boundary integral equation of Stokes flow [23]:

$$\mathbf{v}(\mathbf{x}) = \mathbf{v}^\infty(\mathbf{x}) - \frac{1}{8\pi\mu} \sum_m^M \int_{A_m} \mathbf{J}^E \cdot \mathbf{q}(\mathbf{y}) dA(\mathbf{y}), \quad (1)$$

where $\mathbf{v}^\infty = \dot{\gamma}x_2\mathbf{e}_1$ is the undisturbed flow, m is the index of capsules, A_m is the surface of capsule m , and \mathbf{q} is the traction jump across the membrane. For an infinite periodic domain, the Ewald summation proposed by Beenakker [24] is used, where the summation is decomposed into the summation of a real space and that of a reciprocal space. The Green's function \mathbf{J}^E is then given by

$$\begin{aligned} J_{ij}^E &= \sum_\gamma J_{ij}^{E_I}(\mathbf{r}_\gamma) + \frac{8\pi}{V} \sum_{\lambda \neq 0} J_{ij}^{E_{II}}(\mathbf{k}_\lambda), \quad J_{ij}^{E_I} = \frac{\delta_{ij}}{r} E_1 + \frac{r_i r_j}{r^3} E_2, \\ J_{ij}^{E_{II}} &= \left(\frac{\delta_{ij}}{k^2} - \frac{k_i k_j}{k^4} \right) \left(1 + \frac{k^2}{4\xi^2} + \frac{k^4}{8\xi^4} \right) \exp\left(-\frac{k^2}{4\xi^2} \right) \cos(\mathbf{k} \cdot \mathbf{r}), \end{aligned}$$

and

$$E_1 = \operatorname{erfc}(\xi r) + \frac{\exp(-\xi^2 r^2)}{\sqrt{\pi}}(4\xi^3 r^3 - 6\xi r),$$

$$E_2 = \operatorname{erfc}(\xi r) + \frac{\exp(-\xi^2 r^2)}{\sqrt{\pi}}(2\xi r - 4\xi^3 r^3),$$

where $V = l_x l_y l_z$ is the volume of the periodic box. The distance vector is given by $\mathbf{r}_\gamma = \mathbf{r}_0 + \mathbf{\Lambda}_\gamma$, where $\mathbf{r}_0 = \mathbf{x} - \mathbf{y}$ and $\mathbf{\Lambda}_\gamma = l_x n_{x\gamma} \mathbf{e}_x + l_y n_{y\gamma} \mathbf{e}_y + l_z n_{z\gamma} \mathbf{e}_z$ ($n_{x\gamma}$, $n_{y\gamma}$, $n_{z\gamma}$ are integer values). The reciprocal lattice vector is given by $\mathbf{k}_\lambda = 2\pi n_{x\lambda} \mathbf{e}_x / l_x + 2\pi n_{y\lambda} \mathbf{e}_y / l_y + 2\pi n_{z\lambda} \mathbf{e}_z / l_z$ ($n_{x\lambda}$, $n_{y\lambda}$, $n_{z\lambda}$ are integer values). $\xi = \pi^{\frac{1}{2}} V^{-\frac{1}{3}}$, $k = |\mathbf{k}|$, and $r = |\mathbf{r}|$. For more details, see Beenakker [24] and Loewenberg and Hinch [25].

The membrane of the capsules is modeled as a two-dimensional isotropic hyperelastic material with negligible bending resistance. The surface deformation gradient tensor \mathbf{F}_s is given by

$$d\mathbf{x} = \mathbf{F}_s \cdot d\mathbf{X}, \quad (2)$$

where $d\mathbf{X}$ and $d\mathbf{x}$ are the infinitesimal vectors in the reference and deformed states, respectively. The Cauchy stress tensor \mathbf{T} is

$$\mathbf{T} = \frac{1}{J_s} \mathbf{F}_s \cdot \frac{\partial w_s}{\partial \mathbf{e}} \cdot \mathbf{F}_s^T, \quad (3)$$

where $J_s = \lambda_1 \lambda_2$ represents the area dilation ratio, λ_1 and λ_2 are the principal extension ratios, w_s is the strain energy function, \mathbf{e} is the Green-Lagrange strain tensor,

$$\mathbf{e} = \frac{1}{2} (\mathbf{F}_s^T \cdot \mathbf{F}_s - \mathbf{I}_s), \quad (4)$$

and \mathbf{I}_s is the tangential projection operator. To reduce the effect of membrane buckling on the macroscopic viscosity, the constitutive law proposed by Skalak *et al.* [26] is used:

$$w_s = \frac{G_s}{2} (I_1^2 + 2I_1 - 2I_2 + CI_2^2), \quad (5)$$

where C is the area dilation constant, $I_1 = \lambda_1^2 + \lambda_2^2 - 2$, and $I_2 = J_s^2 - 1$. Lac *et al.* [27] reported that a capsule with a Skalak membrane did not have membrane buckling for a relatively wide range of the capillary number, $0.4 \leq \text{Ca} \leq 2.4$, even without bending resistances.

The equilibrium condition between the traction \mathbf{q} and the Cauchy stress \mathbf{T} is given in the weak form as

$$\int_A \hat{\mathbf{u}} \cdot \mathbf{q} dA = \int_A \hat{\mathbf{e}} : \mathbf{T} dA, \quad (6)$$

where $\hat{\mathbf{u}}$ is the virtual displacement, $\hat{\mathbf{e}}$ is the virtual strain, and the kinematic condition is

$$\frac{d\mathbf{x}}{dt} = \mathbf{v}(\mathbf{x}). \quad (7)$$

We calculate the specific viscosity μ_{sp} that indicates the increased viscosity due to the presence of capsules:

$$\mu_{sp} = \frac{\Sigma_{12}^{(p)}}{\mu \dot{\gamma}}. \quad (8)$$

Σ is the particle stress tensor defined by

$$\Sigma^{(p)} = n^A \langle \mathbf{S}^A \rangle + n^B \langle \mathbf{S}^B \rangle, \quad (9)$$

$$\mathbf{S} = \int_A \frac{1}{2} (\mathbf{x} \otimes \mathbf{q} + \mathbf{q} \otimes \mathbf{x}) dA, \quad (10)$$

where n is the number density of capsules, \mathbf{S} is the stresslet tensor, and angle brackets $\langle \rangle$ indicate the ensemble average [28].

C. Numerical simulation

The finite element method for membrane mechanics is coupled with the boundary element method for fluid mechanics [29]. Equation (6) is solved by the finite element method. The direct integral of Eq. (1) for the whole capsules requires heavy computational load. We employ multipole expansion [23,30]. Consider the membrane of a capsule that is composed of P patches of element groups [10,31]. The disturbed velocity generated by capsule m in the far field is then written as

$$\delta v_i^m(\mathbf{x}) = -\frac{1}{8\pi\mu} \sum_p^P \{J_{ij}^E F_j^{mp} + R_{ij}^E L_j^{mp} + K_{ijk}^E S_{jk}^{mp} + O(r^{-3})\}, \quad (11)$$

$$F_i^{mp} = \int_{A^{mp}} q_i(\mathbf{y}) dA(\mathbf{y}), \quad (12)$$

$$L_i^{mp} = \int_{A^{mp}} \varepsilon_{ijk} \hat{r}_j q_k dA(\mathbf{y}), \quad (13)$$

$$S_{ij}^{mp} = \frac{1}{2} \int_{A^{mp}} \left\{ \hat{r}_i q_j(\mathbf{y}) + \hat{r}_j q_i(\mathbf{y}) - \frac{2}{3} \delta_{ij} \hat{r}_k q_k(\mathbf{y}) \right\} dA(\mathbf{y}), \quad (14)$$

where \mathbf{F}^{mp} is the force, \mathbf{L}^{mp} is the torque, \mathbf{S}^{mp} is the stresslet, and A^{mp} is the surface area of the p th patch of the capsule, and $\hat{\mathbf{r}}$ is the vector from the center of patch p to the observation point \mathbf{x} . The two propagators are given by

$$R_{ij}^E = \frac{1}{4} \varepsilon_{kjl} (\nabla_k J_{ij}^E - \nabla_l J_{ij}^E), \quad (15)$$

$$K_{ijk}^E = \frac{1}{2} (\nabla_k J_{ij}^E + \nabla_j J_{ik}^E). \quad (16)$$

In this study, the membrane of each capsule consists of 1280 triangular elements ($N_E = 1280$). The Gaussian quadrature method is used for the integral of Eq. (1) for $r/a < 3$, where polar coordinates are introduced for singular elements [4]. For Eq. (11), the number of patches is set to $P = 80$ for $3 \leq r/a < 10$ and $P = 20$ for $r/a \geq 10$, where each patch has $1280/80 = 18$ elements and 64 elements for $P = 80$ and $P = 20$, respectively. While semi-implicit methods have been also used for the time integration (for example, see Rahimian *et al.* [32]), the second-order explicit Runge-Kutta method is used in this study, and all the procedures are fully implemented in graphics processing unit computing. For more detail, please see Matsunaga *et al.* [33] and Matsunaga *et al.* [10].

The numerical method has been successfully applied to investigate the rheology of a monomodal capsule suspension in simple shear flow [10]. In this previous study, we checked the effects of the mesh size, the initial positions of the capsules, and the number of capsules per unit domain on the shear viscosity of the capsule suspension. Similar tests are also examined for a bimodal suspension. Because our interest is the shear viscosity at quasisteady states, the initial positions of the capsules are randomly given. Three cases with different initial capsule positions are simulated for $N_E = 1280$ and $N_E = 5120$. The temporal values of the specific viscosity are shown in Fig. 2(a) for $R_\phi = 0.5$, $R_a = 0.5$, $R_{Ca} = 1$, and $Ca^A = 0.4$, where we take only the spatial average to have the temporal values. The transient phase is finished within $\dot{\gamma}t < 10$. Hereafter, we set the starting time to be $\dot{\gamma}t_s = 10$ to exclude the transient phase. Figure 2(b) shows the ensemble average of the specific viscosity as a function of the total length of the simulation t_e , where the time averaging is performed for $t_s \leq t \leq t_e$. There is only a small difference in the values among the cases, particularly for $\dot{\gamma}t_e > 40$. We also examine the effect of the number of capsules in Fig. 2(c). The specific viscosity nearly converges for $M \geq 100$. In this study, we set $N_E = 1280$, $t_e = 100$, $M \geq 100$, and three cases are simulated for each case with different initial positions.

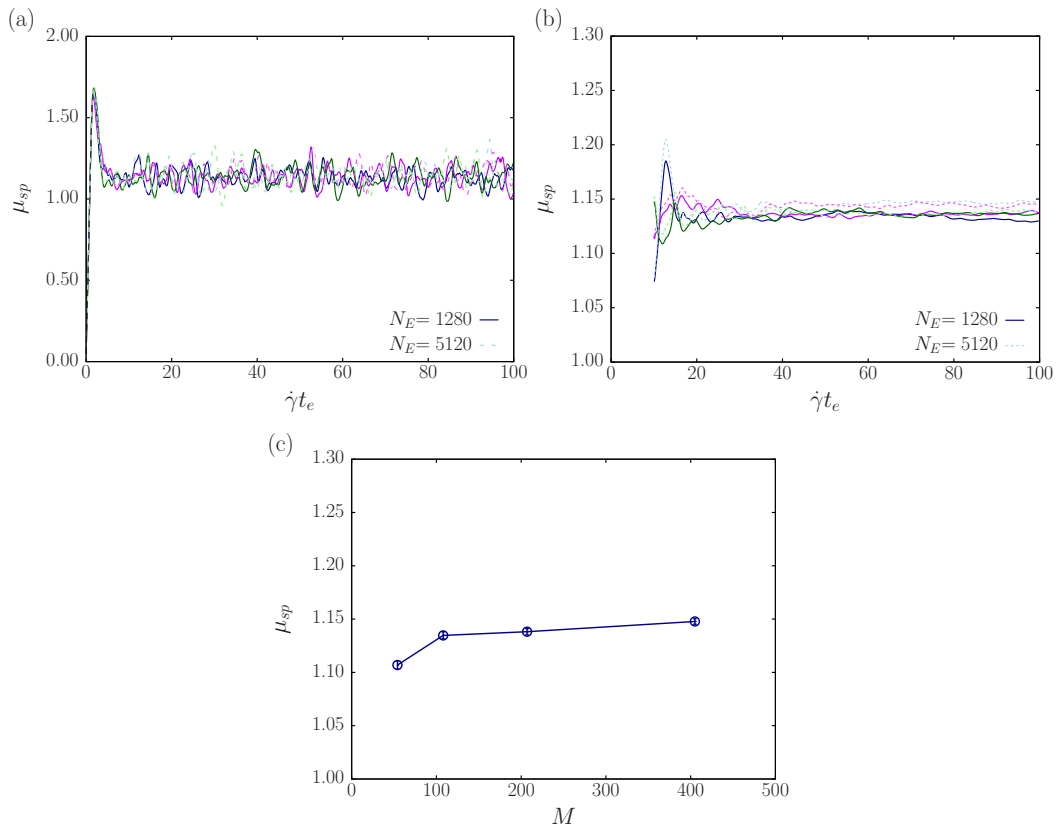


FIG. 2. (a) The temporal value of the specific viscosity, where we take only the spatial average. Three cases with different initial positions, represented by different line colors, are simulated for each mesh size. The transient phase is finished within $\dot{\gamma}t < 10$. (b) Effects of the mesh size (the number of elements per capsule N_E) and the ending time t_e on the ensemble average of the specific viscosity. Different line colors show different initial capsule positions. (c) Effect of the number of capsules on the specific viscosity, where the error bars show the standard deviations of the three cases. Parameters are $R_\phi = 0.5$, $R_a = 0.5$, $R_{Ca} = 1$, and $Ca^A = 0.4$.

III. RESULTS

A. Suspension of capsules with different sizes

First, we analyze a bimodal suspension of two types of capsules with different sizes and the same deformability. The radius and capillary number ratios are set to $R_a = 0.5$ and $R_{Ca} = 1$, with the capsules of type A referring to large capsules and type B to small capsules. To investigate the effects of the deformability of the capsules on the shear viscosity, three values of the capillary number are examined. The specific viscosity is presented in Fig. 3(a) for various values of the volume ratio R_ϕ . Because the small capsules have the same capillary number as the large capsules, $Ca^B = Ca^A$, monomodal suspensions have a constant viscosity between $R_\phi = 0$ and $R_\phi = 1$. Shear-thinning behavior in the shear viscosity [3] is also found in bimodal capsule suspensions. In addition, the specific viscosity of a bimodal suspension is lower than that of corresponding monomodal suspension for $0 < R_\phi < 1$.

To evaluate the extent of the viscosity reduction, we simply compare the viscosity of a bimodal suspension, μ_{sp} , with that of the corresponding monomodal suspensions,

$$\mu_{sp}^* = \mu_{sp}|_{R_\phi=0} = \mu_{sp}|_{R_\phi=1}. \quad (17)$$

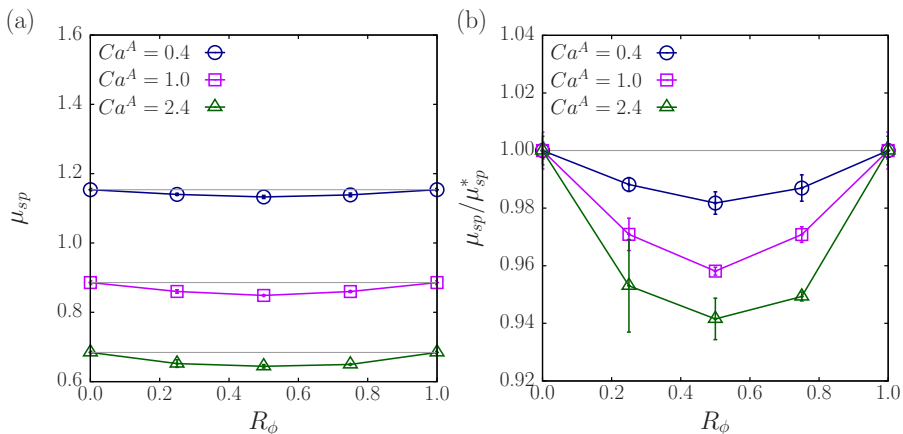


FIG. 3. (a) Specific viscosity μ_{sp} and (b) its ratio to that of monomodal suspensions μ_{sp}^* for $R_a = 0.5$ and $R_{Ca} = 1$.

In Fig. 3(b) we find that the shear viscosity of the bimodal capsule suspensions exhibits a viscosity reduction, with a larger reduction for a higher capillary number. This result clearly suggests that the extent of the viscosity reduction is amplified by the deformability of particles.

The viscosity reduction must result from a reduction in the shear component of the stresslet of the capsules, S_{12} , but it is unclear whether the values of S_{12} are reduced for both the large and small capsules, or whether they exhibit different behaviors. Therefore, we analyze the stresslet separately for large and small capsules. In Fig. 4 we see that the ensemble average of the stresslet for large capsules behaves differently from that for small capsules. The stresslet of the large capsules is smaller in a bimodal suspension than the monomodal suspension and decreases with increasing R_ϕ . A stronger reduction is also found at a higher capillary number. For the small capsules, however, the stresslet for a bimodal suspension shows a value slightly larger than that for the monomodal suspension.

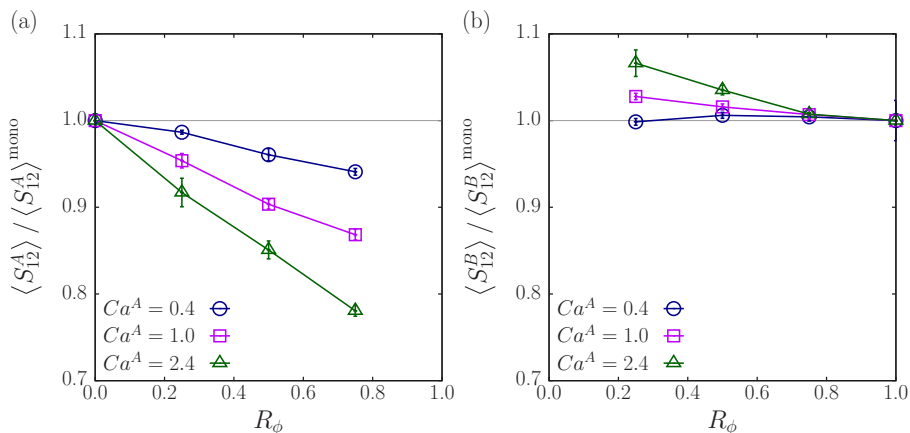


FIG. 4. Shear component of the stresslet S_{12} for $R_a = 0.5$ and $R_{Ca} = 1$. Ensemble average for (a) large capsules (type A) and (b) small capsules (type B). The values are normalized by those for monomodal suspensions, denoted by the superscript “mono.”

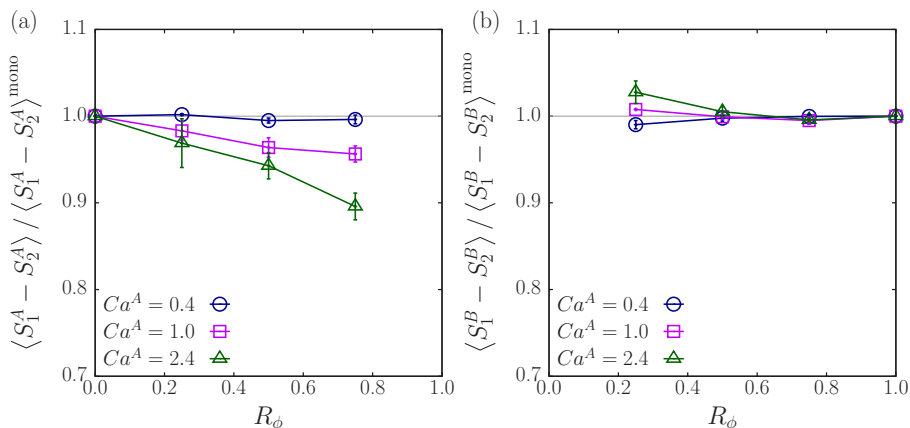


FIG. 5. Principal stresslet difference $S_1 - S_2$ for $R_a = 0.5$ and $R_{Ca} = 1$. Ensemble average for (a) large capsules (type A) and (b) small capsules (type B).

The microstructure of suspensions is often discussed in the study of the rheology of rigid-particle suspensions, and the deformation and orientation of capsules greatly affect the microstructure of capsule suspensions [8]. We thus consider the effects of the deformation and orientation of the capsules on the stresslet behaviors [10]. For the ensemble average, the following approximation may be applicable:

$$\langle S_{12} \rangle \approx \frac{1}{2} \langle S_1 - S_2 \rangle \sin 2\langle \theta_S \rangle, \quad (18)$$

where S_1 and S_2 are the principal values of the stresslet (eigenvalues) in the shear plane, and θ_S is the orientation angle of the stresslet with respect to the flow direction. The principal stresslet difference $S_1 - S_2$ represents the strength of the stresslet due to the deformation of the capsule, and $\sin 2\theta_S$ is due to the orientation of the capsule. Note that the stresslet angle θ_S is not a direct measure of the orientation of the capsules. In a previous study [10], we investigated the relationship between the stresslet angle and the orientation angle, and we confirmed that these angles had nearly one-to-one correspondence. Figure 5 shows the principal stresslet difference for the large and small capsules. For the large capsules, the principal stresslet difference decreases with increasing R_ϕ ,

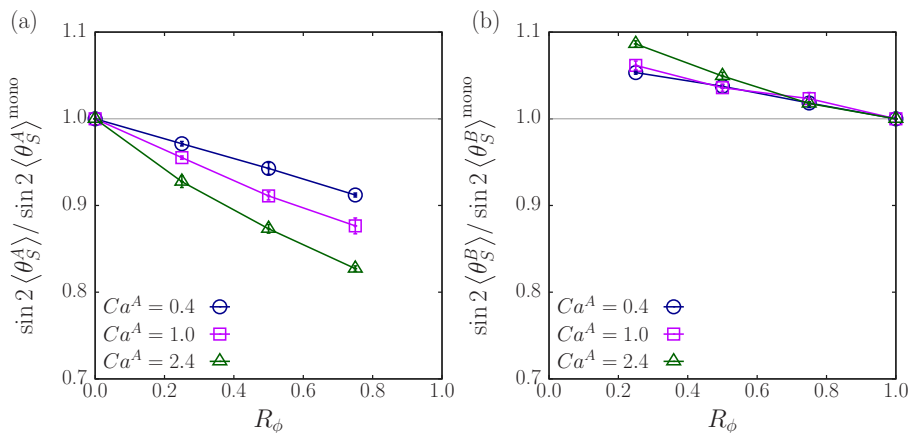


FIG. 6. The value of $\sin 2\theta_S$ for $R_a = 0.5$ and $R_{Ca} = 1$. Ensemble average for (a) large capsules (type A) and (b) small capsules (type B).

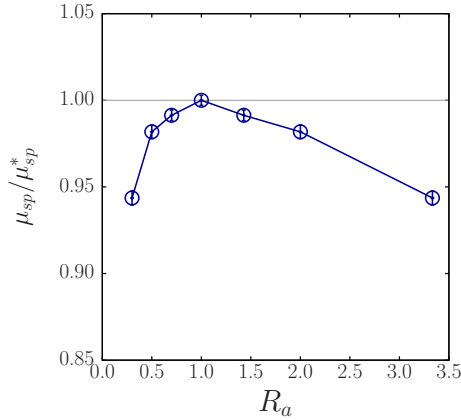


FIG. 7. Effect of the size ratio R_a on the specific viscosity, where $R_\phi = 0.5$, $R_{Ca} = 1$, and $Ca^A = 0.4$.

in particular, for $Ca = 1$ and $Ca = 2.4$. In contrast, the principal stresslet difference for the small capsules is comparable to that for the monomodal suspension. The value of $\sin 2\langle\theta_S\rangle$ is presented in Fig. 6. The value for the large capsules also decreases when R_ϕ increases, while that for the small capsules slightly increases with $1 - R_\phi$. It should be also noted that the effect of the orientation of the capsules on the stresslet is larger than that of the deformation. These results suggest that the orientation angle of the large capsules with respect to the flow direction, as well as their deformation, is decreased by interacting with the small capsules. These effects decrease the shear component of the stresslet for the large capsules and consequently cause the viscosity reduction of the bimodal capsule suspensions.

We also examine the effects of the size ratio on the shear viscosity. Figure 7 shows the specific viscosity for various values of R_a , where $R_\phi = 0.5$, and $Ca^A = 0.4$. For convenience, the viscosity values are plotted not only for $R_a \leq 1$ but also for $R_a > 1$. As shown in this figure, the extent of the viscosity reduction increases with the size difference.

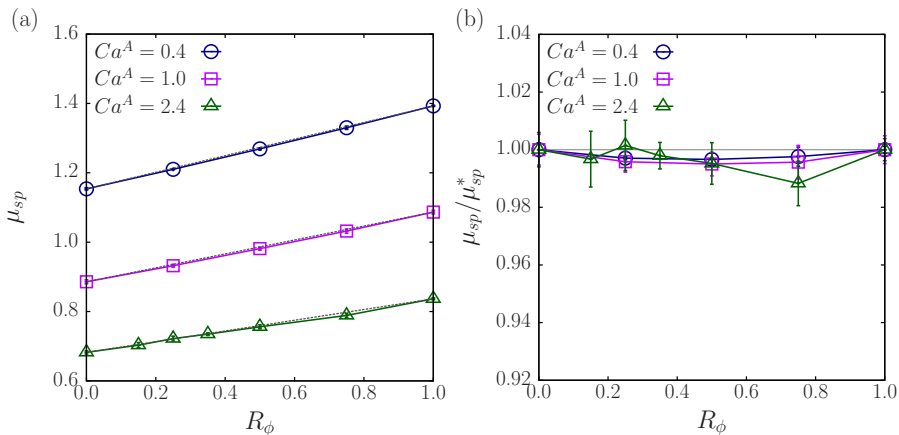


FIG. 8. (a) Specific viscosity μ_{sp} and (b) its ratio to the weighted average for monomodal suspensions μ_{sp}^* for $R_a = 1$ and $R_{Ca} = 0.5$.

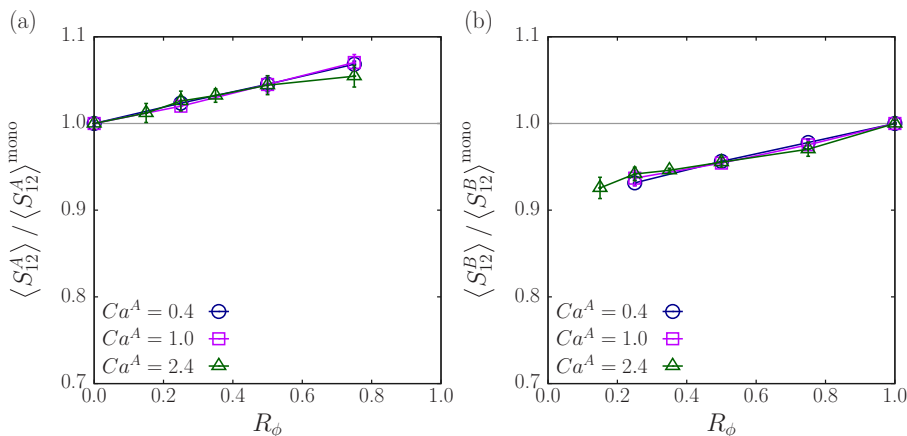


FIG. 9. Shear component of the stresslet S_{12} for $R_a = 1$ and $R_{Ca} = 0.5$. Ensemble average for (a) floppy capsules (type A) and (b) stiff capsules (type B).

B. Suspension of capsules with different deformabilities

Next, we consider a bimodal suspension of two types of capsules with the same size and different deformabilities, $R_a = 1$ and $R_{Ca} = 0.5$. The capsules of type A are floppy capsules, and those of type B are stiff capsules. The specific viscosity is shown in Fig. 8(a) for three values of the capillary number for the floppy capsules. Because the capillary number of the stiff capsules is lower than that of the floppy capsules, the specific viscosity at $R_\phi = 0$ is lower than that at $R_\phi = 1$ due to the shear-thinning effect. To compare the shear viscosity of a bimodal suspension with the corresponding monomodal suspensions, we simply use a weighted average between the values at $R_\phi = 0$ and $R_\phi = 1$:

$$\mu_{sp}^* = (1 - R_\phi)\mu_{sp}|_{R_\phi=0} + R_\phi\mu_{sp}|_{R_\phi=1}. \quad (19)$$

As shown in Fig. 8(b), the specific viscosity of the bimodal suspensions is nearly the same value as the weighted average of the monomodal suspensions. Note that because there is a relatively large deviation, we examined six cases and also added the data at $R_\phi = 0.15$ and 0.3 for $Ca = 2.4$.

To examine whether the shear component of the stresslet also takes the same value as that in the monomodal suspensions, we analyze the stresslet behaviors separately for the floppy and stiff capsules. In Fig. 9 we see that S_{12} for each type of capsule in a bimodal suspension takes a different value from the monomodal suspension. The stresslet for the floppy capsules increases with R_ϕ , whereas that for the stiff capsules decreases when $1 - R_\phi$ increases, though the extent of the change is not large, and the dependency on the capillary number is not observed.

To consider the effects of the deformation and orientation of each type of capsule on the behavior of their stresslets, the principal stresslet difference and the orientation angle of the stresslet relative to the flow direction are shown in Figs. 10 and 11, respectively. We find that the changes in the shear component of the stresslet are mainly caused by changes in the principal stresslet difference, while the orientation angle remains nearly constant. In the case of a bimodal suspension of two types of capsules with the same size and different deformabilities, the deformation of the floppy capsules increases and that of the stiff capsules decreases. An increase in the stresslet of the floppy capsules is counterbalanced by a decrease in the stresslet of the stiff capsules, and the resultant shear viscosity is nearly the same as the weighted average of their monomodal suspensions.

Figure 12 shows the effect of the capillary number ratio on the specific viscosity. The dependency on the capillary number ratio is small. Although there is a small viscosity reduction for $R_{Ca} \ll 1$, the specific viscosity still takes a value similar to the weighted average of the monomodal suspensions in the examined range of R_{Ca} .

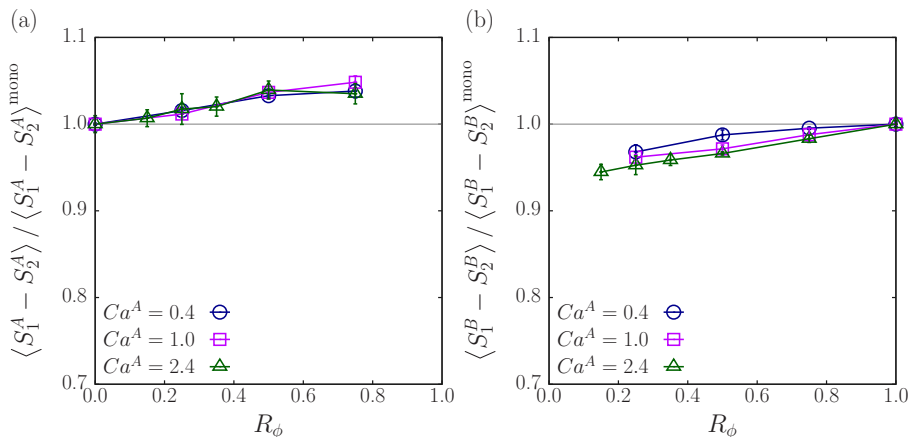


FIG. 10. Principal stresslet difference $S_1 - S_2$ for $R_a = 1$ and $R_{Ca} = 0.5$. Ensemble average for (a) floppy capsules (type A) and (b) stiff capsules (type B).

C. Suspension of capsules with different sizes and the same membrane stiffness

Finally, we discuss a suspension of two types of capsules with different sizes and the same membrane stiffness, $R_a = 0.5$ and $R_G = 1$. This type of bimodal suspension could be found in the production of artificial capsules, for example, if the membranes of large and small capsules are composed of the same material with the same thickness. As shown in Sec. III A, the size difference of the two types of capsules induces a decrease in the deformation of large capsules as well as a decrease in the orientation angle relative to the flow direction. This causes a reduction in the shear component of the stresslet of the large capsules and is a direct cause of the viscosity reduction. Here the capsules of two sizes have the same membrane stiffness, and therefore the large capsules must be floppier than the small capsules, $R_{Ca} = R_a = 0.5$. In a suspension of two types of capsules with different deformabilities, however, the stresslet of the floppy capsules instead increases relative to the weighted average of the monomodal suspensions. The same effect of the deformability difference is also expected for a suspension of capsules with different sizes and the same membrane stiffness and may suppress the extent of the viscosity reduction.

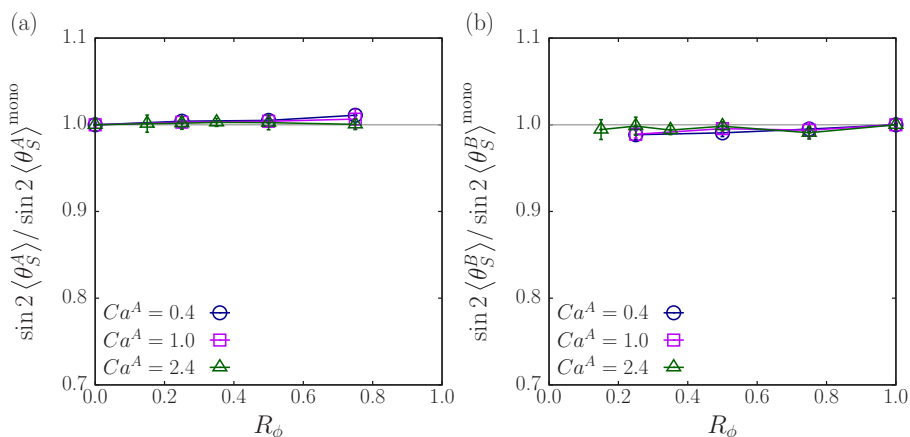


FIG. 11. The value of $\sin 2\theta_S$ for $R_a = 1$ and $R_{Ca} = 0.5$. Ensemble average for (a) floppy capsules (type A) and (b) stiff capsules (type B).

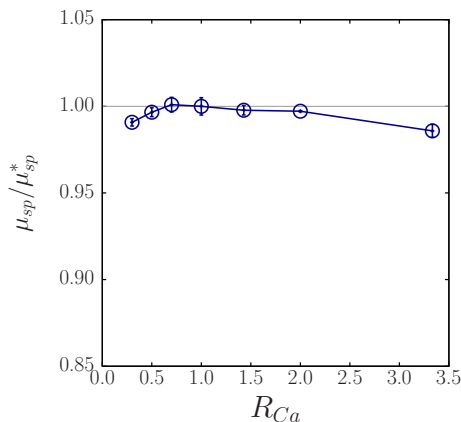


FIG. 12. Effect of the capillary number ratio R_{Ca} on the specific viscosity, where $R_\phi = 0.5$, $R_a = 1$, and $Ca^A = 0.4$.

Figure 13 shows the specific viscosity of several bimodal suspensions, along with the weighted average of the corresponding monomodal suspensions. The viscosity reduction is confirmed for various values of Ca^A , and the extent of the viscosity reduction further increases compared with the suspension of capsules with different sizes and the same deformability (Fig. 3). The shear component of the stresslet for the large and small capsules is also shown in Fig. 14. The stresslet of the large capsules shows the same tendency as observed for a suspension of capsules with different sizes (Fig. 4), but the stresslet for the small capsules instead decreases from the weighted average of monomodal suspensions.

To understand the interplay of the size and deformability differences on the stresslet behaviors, we examine how the deformation and orientation angle of the capsules change in the bimodal suspensions. As shown in Fig. 15, the principal stresslet difference of the large capsules increases, and that of the small capsules decreases. The principal stresslet difference does not show the same tendency as a suspension of capsules with different sizes (Fig. 5), but instead resembles a suspension of capsules with different deformabilities (Fig. 10). In contrast, as shown in Fig. 16, the trend of

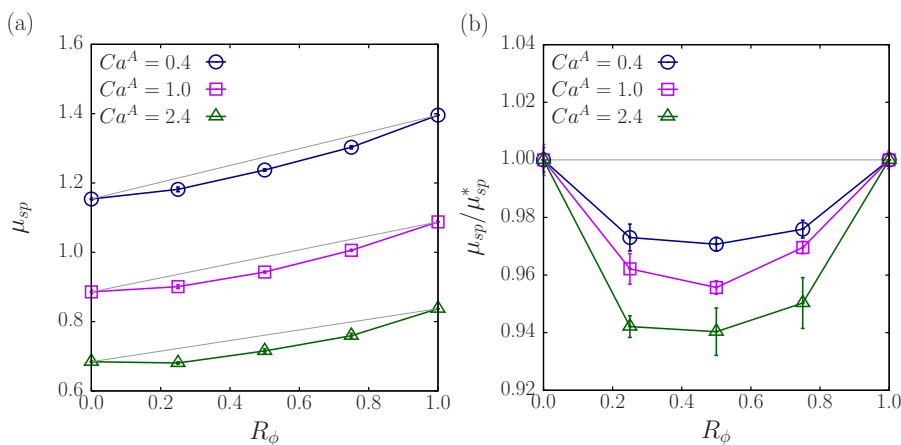


FIG. 13. (a) Specific viscosity μ_{sp} and (b) its ratio to the weighted average of monomodal suspensions μ_{sp}^* for $R_a = 0.5$ and $R_G = 1$ ($R_{Ca} = 0.5$).

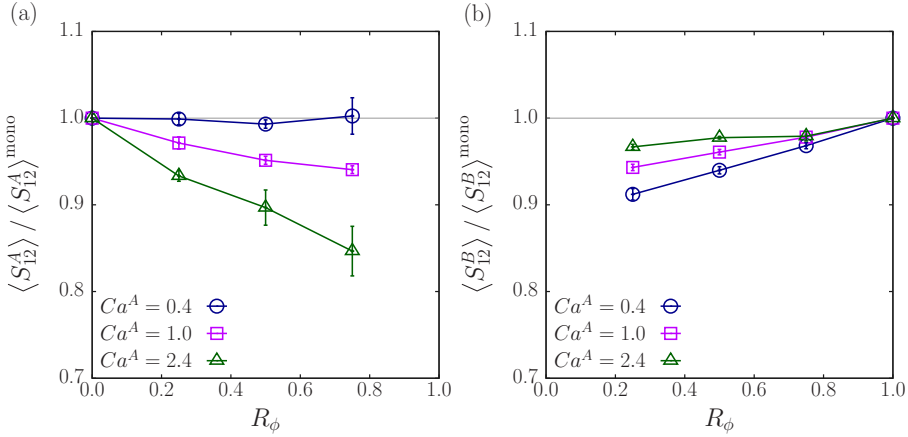


FIG. 14. Shear component of the stresslet S_{12} for $R_a = 0.5$ and $R_G = 1$ ($R_{Ca} = 1$). Ensemble average for (a) large capsules (type A) and (b) small capsules (type B).

$\sin 2\theta_S$ is qualitatively similar to a suspension of capsules with different sizes (Fig. 6), in which the orientation angle of the large capsules decreases and that of the small capsules increases.

These results suggest that the size difference mainly affects the orientation angle of the capsules, and that the deformability difference affects the deformation of the capsules. For a suspension of two types of capsules with different sizes and the same membrane stiffness, these effects coexist. The interplay between the size and deformability differences decreases the stresslet for both the large and small capsules, resulting in a further viscosity reduction.

This is also confirmed in Fig. 17, where the specific viscosity is plotted as a function of R_a (R_{Ca}) for $R_\phi = 0.5$, and $Ca^A = 0.4$. As observed for a bimodal suspension with a size difference (Fig. 7), a viscosity reduction appears, and a stronger reduction is expected for a larger difference in the capsule sizes.

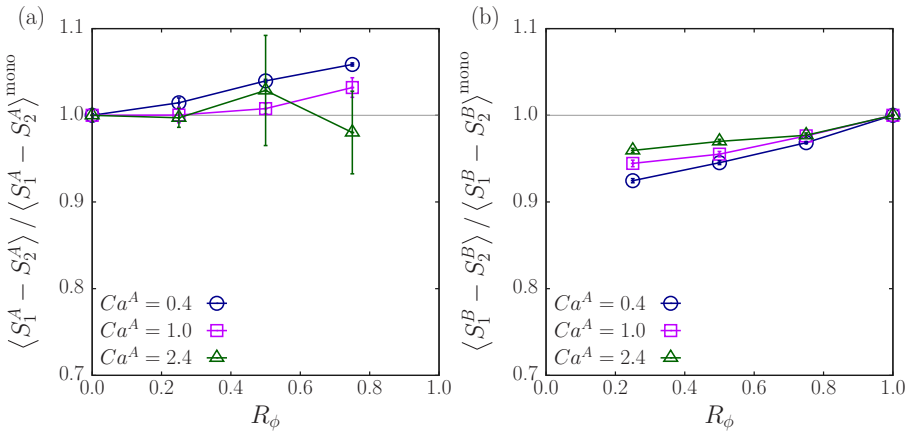


FIG. 15. Principal stresslet difference $S_1 - S_2$ for $R_a = 0.5$ and $R_G = 1$ ($R_{Ca} = 0.5$). Ensemble average for (a) large capsules (type A) and (b) small capsules (type B).

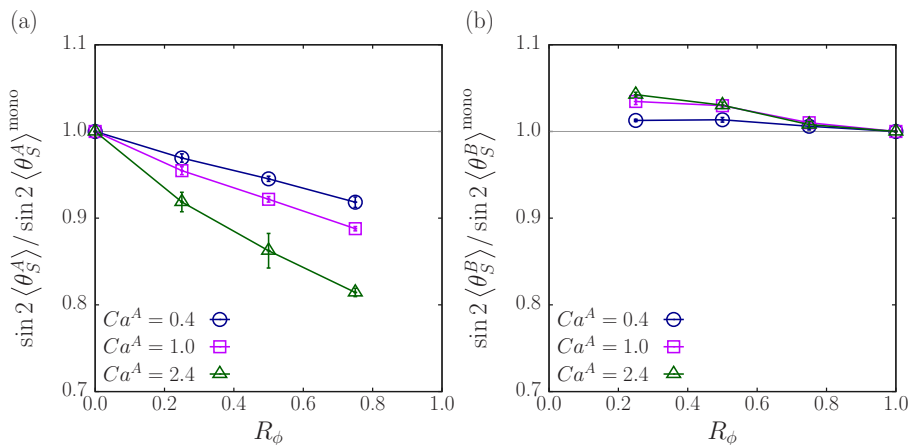


FIG. 16. The value of $\sin 2\theta_S$ for $R_a = 0.5$ and $R_G = 1$ ($R_{Ca} = 0.5$). Ensemble average for (a) large capsules (type A) and (b) small capsules (type B).

IV. DISCUSSION

The characteristic rheological behavior of bimodal suspensions of rigid particles is a reduction in shear viscosity. The shear viscosity is lower for a suspension of two sizes of rigid particles than a monomodal suspension of small/large particles [12,13]. Most previous studies concentrated on bimodal suspensions of rigid particles. Although a few studies investigated the viscosity reduction in bimodal emulsions [18–20], the effect of the particle deformability on this phenomenon has not been fully understood. The primary objective of this study was thus to clarify whether the deformability of particles amplifies the extent of viscosity reduction or suppresses it. For this objective, we have performed a numerical analysis of the shear viscosity of bimodal capsule suspensions in simple shear flow under the Stokes flow regime. First, we have analysed the shear viscosity of a suspension of two types of capsules with different sizes and the same deformability. As expected, the bimodal capsule suspension has a decreased shear viscosity compared to monomodal capsule suspensions. In addition, a finding of this study is that the extent of the viscosity reduction is amplified by the deformability of capsules. A larger viscosity reduction appears at a higher capillary number. We

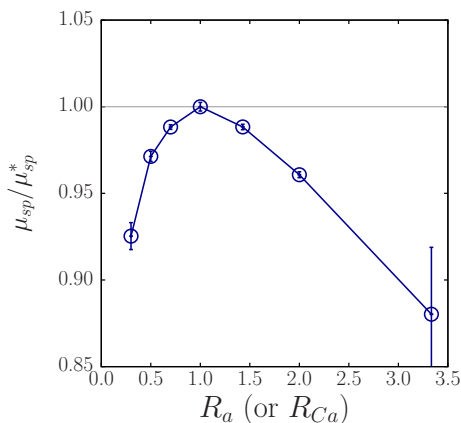


FIG. 17. Effect of the size ratio (the capillary number ratio) on the specific viscosity, where $R_\phi = 0.5$, $R_G = 1$, and $Ca^A = 0.4$.

fixed the total volume fraction of capsules to be $\phi = 0.4$. In previous studies of bimodal suspensions of rigid particles, the viscosity reduction was not significant for such a moderate volume fraction [12]. When $Ca^A \rightarrow 0$, the specific viscosity of a bimodal capsule suspension is expected to converge to that of a rigid particle suspension. However, when the capillary number increases to $Ca^A = 2.4$, the viscosity reduction reaches more than 5% even for $R_a = 0.5$. The reduction rate is still not large, but the results clearly show a qualitative trend of the enhanced viscosity reduction due to the deformability. This would be of practical importance if the volume fraction becomes larger. It was reported that the extent of the viscosity reduction increased with the total volume fraction of the rigid particles. The extent of the viscosity reduction also increased with the size difference of the rigid particles. Consequently, at $\phi = 0.6$ and $R_a = 0.138$, for example, the viscosity of a bimodal rigid-sphere suspension was one order of magnitude smaller than that of a monomodal suspension [13,14]. Although we were not able to examine such a high volume fraction due to numerical limitations, a further viscosity reduction is expected for bimodal capsule suspensions. We also showed that the size difference mainly affects the orientation angle of the capsules. The orientation angle with respect to the flow direction decreases for the large capsules, and the viscosity reduction is mainly caused by a decrease in the stresslet for the large capsules.

In practical applications, two sizes of capsules may have the same membrane stiffness. This category of bimodal capsule suspensions resembles bimodal emulsions. The viscosity reduction was also reported in previous studies on bimodal emulsions [18–20]. However, a larger droplet must have a higher capillary number, and the separate effects of the size and deformability differences on the shear viscosity remain unclear. To clarify the separate effects of the size and deformability differences and their interplay, next, we have analyzed a suspension of capsules with the same size and different deformabilities. In this case, the specific viscosity of a bimodal suspension is nearly the same as the weighted average of monomodal suspensions. The deformability difference mainly affects the deformation of the capsules. However, a decrease in the stresslet for the stiff capsules is counterbalanced by an increase in the stresslet for the floppy capsules, and a substantial viscosity reduction is not observed. Finally, we have analysed a suspension of capsules with different sizes and the same membrane stiffness. As expected, the effects of both the size and deformability differences are observed. The interplay of these effects decreases the stresslet for both the large and small capsules, resulting in a further viscosity reduction. The same mechanism is also expected for bimodal emulsions.

There are many parameters in bimodal capsule suspensions, and we have concentrated on the size ratio and capillary number ratio in this study. For example, a recent experiment [21] showed that the surface shear elastic modulus G increased nonlinearly with the capsule size. This experiment suggests that we must consider both the size ratio and the capillary number ratio for general bimodal suspensions. Other parameters, including the viscosity ratio between the outer and inner liquids and the bending stiffness of the membrane affect the shear viscosity. These parameters also change the capsule deformability, and they are expected to exhibit a similar effect to the capillary number ratio. It is also interesting to study the effect of the capsule resting shape and the inertial effect on the viscosity reduction. For example, a previous study [34] showed that the inertia increases the capsule deformation and inclination in planar Poiseuille flow, resulting in a complex behavior of apparent viscosity even for monomodal suspensions. The limitation of this study is that the problem is simplified to gain a fundamental understanding of bimodal capsule suspensions. However, real suspensions are more complex, and further studies are required for a comprehensive understanding of the rheology of bimodal capsule suspensions, in particular for highly concentrated suspensions. We hope that our findings are helpful for future studies.

ACKNOWLEDGMENTS

We thank Dr. Stephanie Nix, Dr. Toshihiro Omori, Prof. Takuji Ishikawa, and Prof. Takami Yamaguchi for helpful discussions. This work was supported by JSPS KAKENHI Grants No. 25000008, No. 17H02075, and No. 18H04100.

- [1] D. Barthès-Biesel, Motion and deformation of elastic capsules and vesicles in flow, *Annu. Rev. Fluid Mech.* **48**, 25 (2016).
- [2] D. Barthès-Biesel and J. M. Rallison, The time-dependent deformation of a capsule freely suspended in a linear shear flow, *J. Fluid Mech.* **113**, 251 (1981).
- [3] D. Barthès-Biesel and V. Chhim, The constitutive equation of a dilute suspension of spherical microcapsules, *Int. J. Multiphase Flow* **7**, 493 (1981).
- [4] C. Pozrikidis, Finite deformation of liquid capsules enclosed by elastic membranes in simple shear flow, *J. Fluid Mech.* **297**, 123 (1995).
- [5] S. Ramanujan and C. Pozrikidis, Deformation of liquid capsules enclosed by elastic membranes in simple shear flow: Large deformations and the effect of fluid viscosities, *J. Fluid Mech.* **361**, 117 (1998).
- [6] P. Bagchi and R. M. Kalluri, Rheology of a dilute suspension of liquid-filled elastic capsules, *Phys. Rev. E* **81**, 056320 (2010).
- [7] J. R. Clausen and C. K. Aidun, Capsule dynamics and rheology in shear flow: Particle pressure and normal stress, *Phys. Fluids* **22**, 123302 (2010).
- [8] J. R. Clausen, D. A. Reasor, and C. K. Aidun, The rheology and microstructure of concentrated non-colloidal suspensions of deformable capsules, *J. Fluid Mech.* **685**, 202 (2011).
- [9] M. Gross, T. Kruger, and F. Varnik, Rheology of dense suspensions of elastic capsules: Normal stresses, yield stress, jamming and confinement effects, *Soft Matter* **10**, 4360 (2014).
- [10] D. Matsunaga, Y. Imai, T. Yamaguchi, and T. Ishikawa, Rheology of a dense suspension of spherical capsules under simple shear flow, *J. Fluid Mech.* **786**, 110 (2016).
- [11] G. Ma, Microencapsulation of protein drugs for drug delivery: Strategy, preparation, and applications, *J. Controlled Release* **193**, 324 (2014).
- [12] R. J. Farris, Prediction of the viscosity of multimodal suspensions from unimodal viscosity data, *Trans. Soc. Rheol.* **12**, 281 (1968).
- [13] J. S. Chong, E. B. Christiansen, and A. D. Baer, Rheology of concentrated suspensions, *J. Appl. Polym. Sci.* **15**, 2007 (1971).
- [14] A. J. Poslinski, Ryan M. E., R. K. Gupta, S. G. Seshadri, and F. J. Frechette, Rheological behavior of filled polymeric systems. II. The effect of a bimodal size distribution of particulates, *J. Rheol.* **32**, 751 (1988).
- [15] C. Chang and R. L. Powell, Dynamic simulation of bimodal suspensions of hydrodynamically interacting spherical particles, *J. Fluid Mech.* **253**, 1 (1993).
- [16] C. Chang and R. L. Powell, Effect of particle size distributions on the rheology of concentrated bimodal suspensions, *J. Rheol.* **38**, 85 (1994).
- [17] K. Qin and A. A. Zaman, Viscosity of concentrated colloidal suspensions: Comparison of bidisperse models, *J. Colloid Interface Sci.* **266**, 461 (2003).
- [18] R. Pal, Effect of droplet size on the rheology of emulsions, *AIChE J.* **42**, 3181 (1996).
- [19] R. Pal, Viscosity and storage/loss moduli for mixtures of fine and coarse emulsions, *Chem. Eng. J.* **67**, 37 (1997).
- [20] M. Ramírez, J. Bullón, J. Andérez, I. Mira, and J.-L. Salager, Drop size distribution bimodality and its effect on O/W emulsion viscosity, *J. Dispersion Sci. Technol.* **23**, 309 (2002).
- [21] J. Gubspun, P.-Y. Gires, C. de Loubens, D. Barthès-Biesel, J. Deschamps, M. Georgelin, M. Leonetti, E. Leclerc, F. Edward-Lévy, and A.-V. Salsac, Characterization of the mechanical properties of cross-linked serum albumin microcapsules: Effect of size and protein concentration, *Colloid Polymer Sci.* **294**, 1381 (2016).
- [22] C. de Loubens, J. Deschamps, F. Edwards-Lévy, and M. Leonetti, Tank-treading of microcapsules in shear flow, *J. Fluid Mech.* **789**, 750 (2016).
- [23] C. Pozrikidis, *Boundary Integral and Singularity Methods for Linearized Viscous Flow* (Cambridge University Press, Cambridge, 1992).
- [24] C. W. J. Beenakker, Ewald sum of the Rotne-Prager tensor, *J. Chem. Phys.* **85**, 1581 (1986).
- [25] M. Loewenberg and J. Hinch, Numerical simulation of a concentrated emulsion in shear flow, *J. Fluid Mech.* **321**, 395 (1996).

- [26] R. Skalak, A. Tozeren, R. P. Zarda, and S. Chien, Strain energy function of red blood cell membranes, [Biophys. J.](#) **13**, 245 (1973).
- [27] E. Lac, D. Barthès-Biesel, N. A. Pelekasis, and J. Tsamopoulos, Spherical capsules in three-dimensional unbounded Stokes flows: Effect of the membrane constitutive law and onset of buckling, [J. Fluid Mech.](#) **516**, 303 (2004).
- [28] G. K. Batchelor, The stress system in a suspension of force-free particles, [J. Fluid Mech.](#) **41**, 545 (1970).
- [29] J. Walter, A.-V. Salsac, D. Barthès-Biesel, and P. Le Tallec, Coupling of finite element and boundary integral methods for a capsule in a Stokes flow, [Intl. J. Numer. Meth. Eng.](#) **83**, 829 (2010).
- [30] L. J. Durlofsky and J. F. Brady, Dynamic simulation of bounded suspensions of hydrodynamically interacting particles, [J. Fluid Mech.](#) **200**, 39 (1989).
- [31] A. Z. Zinchenko and R. H. Davis, A multipole-accelerated algorithm for close interaction of slightly deformable drops, [J. Comput. Phys.](#) **207**, 695 (2005).
- [32] A. Rahimian, S. K. Veerapaneni, D. Zorin, and G. Biros, Boundary integral method for the flow of vesicles with viscosity contrast in three dimensions, [J. Comput. Phys.](#) **298**, 766 (2015).
- [33] D. Matsunaga, Y. Imai, T. Omori, T. Ishikawa, and T. Yamaguchi, A full GPU implementation of a numerical method for simulating capsule suspensions, [J. Biomech. Sci. Eng.](#) **9**, 14-00039 (2014).
- [34] T. Krüger, B. Kaoui, and J. Harting, Interplay of inertia and deformability on rheological properties of a suspension of capsules, [J. Fluid Mech.](#) **751**, 725 (2014).